Lasers in Manufacturing Conference 2025

Micro-welding of thin stainless steel foils using an ultra-short pulsed Laser

Samuel Weber[a,b,1], Mareike Schäfer[a,b], Ellen Bold[c], Sebastian Zimmermann[d], Clarissa Schönecker[d], Egbert Oesterschulze[c], Johannes L'huillier[a,b]

[a]*Institute for Surface and Thin Film Technology (IFOS), Kaiserslautern 67663, Germany*
[b]*Research Center OPTIMAS, Rheinland-Pfälzische Technische Universität Kaiserslautern-Landau (RPTU), Kaiserslautern 67663, Germany*
[c] *Department of Physics, Rheinland-Pfälzische Technische Universität Kaiserslautern-Landau (RPTU), Kaiserslautern 67663, Germany*
[d] *Department of Mechanical and Process Engineering, Rheinland-Pfälzische Technische Universität Kaiserslautern-Landau (RPTU), Kaiserslautern 67663, Germany*

Abstract

The production of practical, miniaturized pipelines that allow liquids to flow smoothly presents numerous challenges. Usually, coatings are applied to the inner walls of the pipe. An innovative approach involves the use of high-precision laser processing. The utilization of USP laser processing is used both to create functional surfaces and to produce miniaturized pipes through a overlap welding process. In the context of the conducted investigations, results on overlap welding with two non-transparent thin foils with ultra-short pulsed lasers are presented in this study. Here, we conducted overlap welding on two 20 µm thin 1.4301 stainless steel foils using a ps laser. Insights into the optimal process parameters and the influence of sample preparation are presented. The parameters are evaluated in terms of power density, weld quality and reduced heat-affected zone (HAZ) of the welding results.
Keywords: micro-welding, ultra-short pulsed laser, overlap welding, thin stainless steel foils

1. Introduction

The fundamental idea of this work is the fabrication of small form factor tubes for liquid transportation. The material utilized for the construction of the tubes is a 20 µm thick stainless steel foil. In general, in order to reduce the friction on the inner side of the walls, a functionalized surface is required. Consequently, a subsequent procedure involving an ultra-short pulsed laser is necessary to achieve the desired surface structure for hydrophobicity. The fabrication of the tubes necessitates the implementation of a welding process. The prevalence of laser welding as a foundational technology in contemporary manufacturing, particularly within the automotive industry, the electronics sector, and the medical technology domain, underscores its significance in modern production processes [1],[2]. This technology offers high process speeds and good joint quality. The utilization of laser welding for the purpose of joining thin metallic or polymer foils, frequently with thicknesses below 100 µm, is a subject that is becoming increasingly demanding. These materials find common applications in battery technology and microfluidic systems [3],[4]. However, the welding of thin foils, typically with a thickness of less than 100 µm, remains challenging. Typically, continuous wave or long pulse lasers are employed. However, these methods can result in excessive heat accumulation, which directly contradicts the minimal heat capacity of thin metal foils. This can result in defects such as burn through or wrapping. The requirement to produce the tubes is utilizing a single laser system without necessitating alterations to the existing configuration when doing the surface functionalization. The use of USP lasers in welding applications has already yielded successful outcomes, particularly in the context of glass-metal

1. Corresponding author. Tel.: +49-631-20573-3455; fax: +49-0631-20573-3003
E-mail address: weber@ifos.uni-kl.de

or glass-glass systems, but not for two thin stainless steel foils [5],[6]. The objective of this study is to establish a set of process parameters that are applicable to the welding of two thin stainless steel foils. A comparative analysis of the weld seams is conducted with regard to their quality and the influence of the heat-affected zone.

2. Experiment

As for the setup a ps ultra-short pulsed laser system Hyper-Rapid 100 355-SW from Coherent Kaiserslautern is used. In the optical setup, the laser beam is magnified by a beam expander with a magnification of three followed by a galvanometric scanner for beam movement. Through an F-Theta optic with a focal length of 255 mm the beam is focused onto the specimen with a minimal spot diameter of 33 µm. The specimen is mounted on an X, Y and rotation axis, and the F-Theta optic can also be adjusted using the Z-axis. For the entirety of the experimental procedure, a wavelength of 532 nm is utilised, with a pulse length of 10 ps and a repetition rate of 1000 kHz. The pulse energy is set at 4.5 µJ.

For the material, we used a 20 µm thick 1.4301 stainless steel foil from Hasberg with a width of 100 mm.

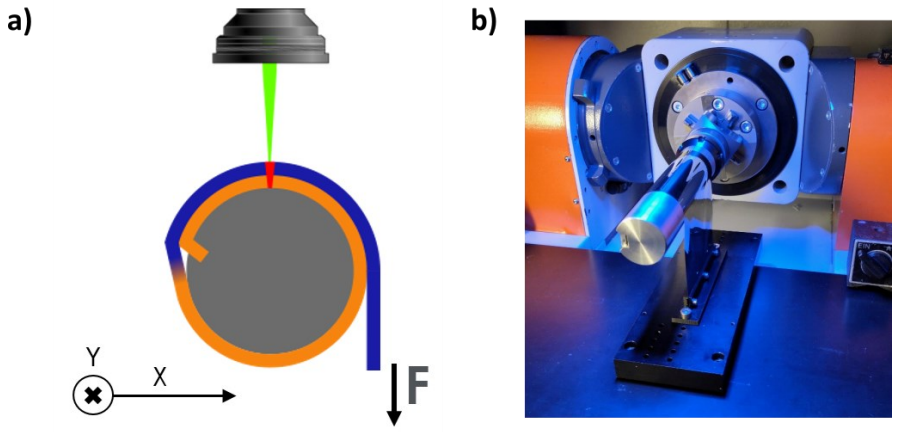

Fig. 1. a) Schematic structure of the specimen holder with a gradient color of the foil to better display the overlaying foils
b) Image from the specimen holder mounted at the rotation axis with the counterweight at the open foil end

As illustrated in Figure 1 a), the specimen holder is used for the purpose of clamping the thin metal foil. The foil is tightly wrapped around the specimen holder, with a diameter of 40 mm. To better distinguish between the two layers of foil, the first layer is colored orange and the second layer is colored blue. On the loose side, the foil is mounted over the complete width of 100 mm on a counterweight with a weight of 2,5 kg. Figure 1 b) shows the specimen holder with the foil and counterweight mounted inside the setup. The objective is to achieve an overlap welding at the uppermost point of the specimen holder on the two layers of thin stainless steel foils. The movement of the laser beam is facilitated by the galvanometer scanner, which operates along the Y-axis of the specimen holder. The length of the weld is 80 mm, resulting in a 10 mm puffer on the edges of the foil length.

The employment of a counterweight is crucial due to the fact that the foil bulges during the welding process, making it impossible to weld the foil. The presence of minor bulges in the foil along the weld's edge persists, even with the incorporation of a counterweight. However, the constant pulling of the foil ensures that the two foils lie on top of each other at the welding point without an air gap.

3. Results and discussion

3.1. Welding performance heat map

A welding performance heat map (see Figure 2) is utilised to defining potential welding parameters. In this investigation, the spot diameter varied by defocusing the laser beam. It starts at the minimum spot diameter at 33 µm (z = 0 mm) and is then increased to 165 µm by shifting the Z-axis to -8 mm. The diameter of the spots located between these points is incremented by z = -2 mm from the smallest diameter. The measurement of the spot diameter is conducted in accordance with the Liu method, utilising the following spot diameters: 33 µm, 48 µm, and 81 µm. It has not been possible to perform a Liu measurement on the -6 mm and -8 mm z-position with a diameter of 128 µm and 164 µm, due to the low fluency at the beam diameter. For these cases the diameter is calculated from the beam angle, as determined by the 81 µm spot diameter. Due to the defocusing this results in the distortion of shape (see beam shape at z = -4 mm and pulse energy of 19 µJ in Appendix Fig. 7.) at the focus spot. The second parameter set is the variation of the welding speed (see Figure 2), which is achieved by the galvanometer scanner. It is determined that the scanner speed is not adjusted to the varying Z positions of the scanner. This is due to the long focusing length, which results in a negligible error occurring at high welding speeds with significant defocusing.

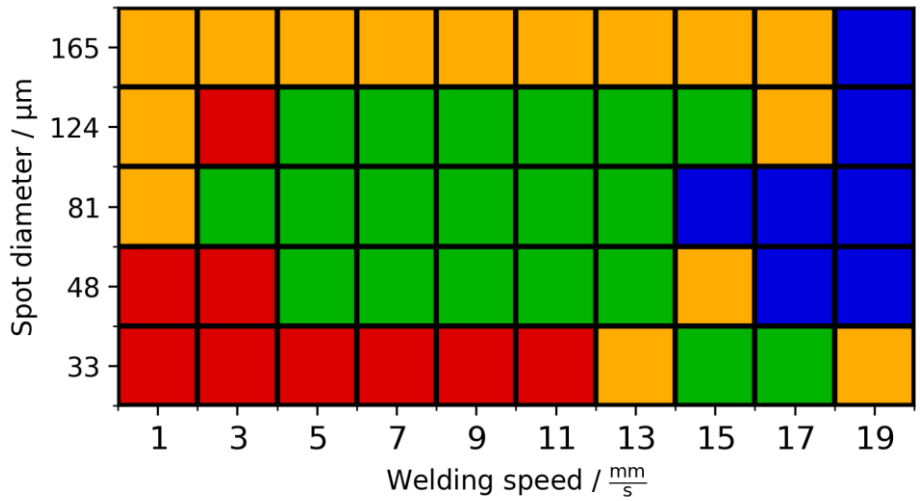

Fig. 2. Welding performance heat map. Blue: No welding, Red: Cut through both foils, Orange: Partly cut / Partly no welding joint, Green: Welded

As illustrated in Figure 2, an evaluation of the parameters associated with the performance of the welding process has been conducted, with particular reference to the condition of the weld seam. The results ranged from a complete cut-through of both metal foils along the entire 80 mm weld line (red), to a total lack of bonding along the weld line (blue). In some cases, partial welds were observed, where certain sections were properly joined, while others were either cut through or not welded at all (orange).The tiles in green show parameter sets, which had a weld over the complete welding line. As expected that in the region with high fluenze and low welding speed both metal foils are cut through while however with faster welding speeds and lower fluence the intensity is not enough to join both metal foils. The area of parameter sets where complete welding was achieved is surrounded by the orange parameters in which the welding process is not stable enough. At the biggest spot diameter, that stable weld is not possible at any welding speed.

In the heat map, a large section of possible welding parameters can be seen, but they differ from each other in terms of welding quality. To analyze the weld quality a cross-section is cut and embedded in resin and ground with a minimum grain size of 8 µm followed by a polishing step with a diamond past of 1 µm grain size. After that, SEM image have been taken with an EVO MA10 from Zeiss. In Figure 3, the area where no welding was performed and the two foils are therefore separated from each other can be seen at the respective edges of the individual images. Due to the difficulty in pouring the resin, which cannot always penetrate the slot between the two foils, this area between the two foils is not clearly visible in Figure 3 a), as residues from the grinding process have settled in this area. For the smallest spot diameter (Figure 3. a)),

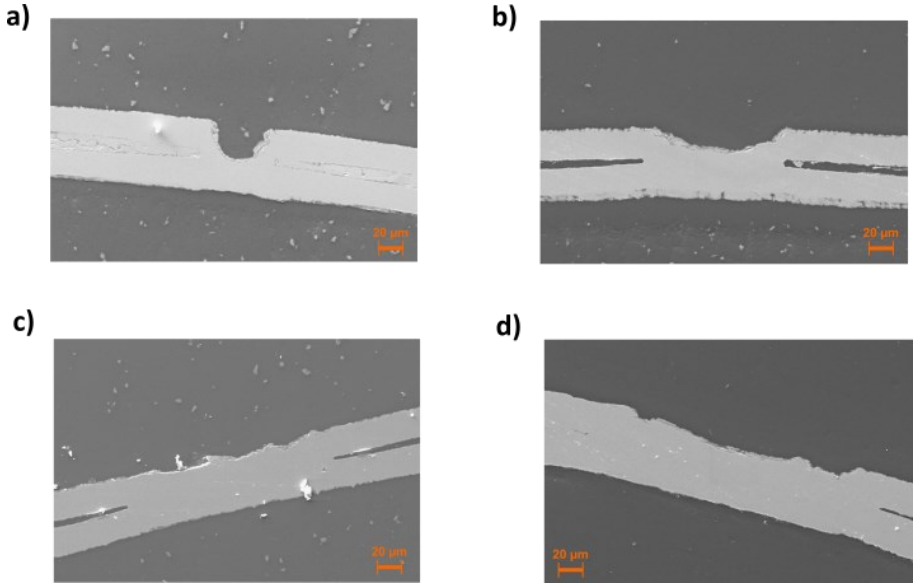

Fig. 3. a) Spot diameter = 33 µm, 17 $\frac{\mathrm{mm}}{\mathrm{s}}$, b) Spot diameter = 48 µm, 9 $\frac{mm}{s}$, c) Spot diameter = 81 µm, 9 $\frac{mm}{s}$, d) Spot diameter $=$ 124 µm, 9 $\frac{mm}{s}$

ablation with a depth of 20 µm takes place due to the high fluence. The upper foil is only connected to the lower foil through molten material at the edge of the ablation. With increasing spot diameter b) -> d), the ablation depth is reduced to only few microns of ablated material. Simultaneously, the width of the welding zone is increased. This becomes most apparent comparing Figure 3 b) and 3 c).

3.2. Weld seam width

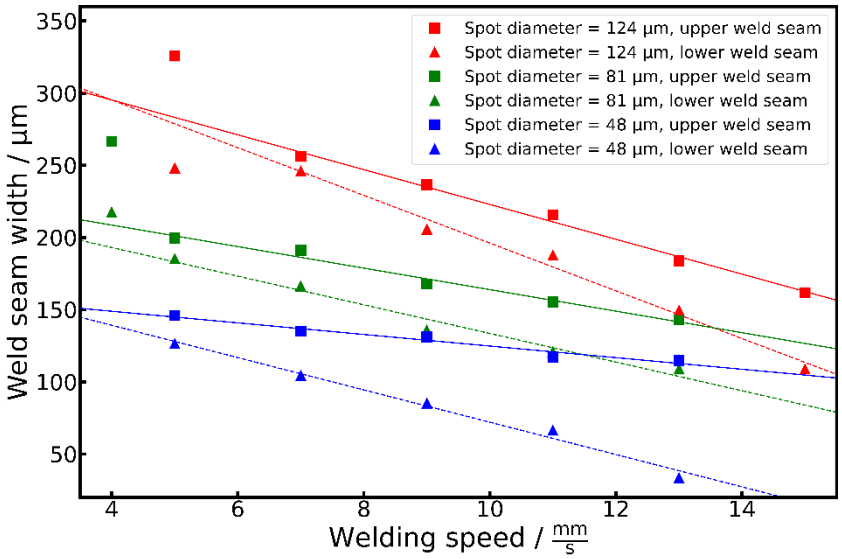

Fig. 4. Weld seam width in dependency of the welding speed

On closer inspection of the weld seam (see Figure 4), there is a difference in the weld seam width of the upper and lower weld seam. The measured region of the weld seam width is the region where the laser spot interacted with the material for the upper side. In contrast, the weld seam width on the lower side reflects the extent of the molten pool. This distinction arises because the laser energy is mostly absorbed at the top surface and then conducted through the material, influencing the melt pool formation beneath. The measured region can be seen in the Appendix in Figure 8 as an example for an upper and lower weld seam width. For the assessment of the weld width, the welds with a spot diameter of 33 µm have not been investigated due to the high ablation rate which exceeds the depth of the thickness of the first foil. The error bars were omitted from the graphs, as they would impair the clarity of the graph due to the small span. For the linear interpolation of

the upper and lower weld seam widths, the results for the slowest welding speed, specifically for spot diameters of 124 µm and 81 µm, were not included in the analysis. These particular welds exhibited inconsistent seam widths along the weld line. Such irregularities are likely due to the fact that these parameter combinations lie at the boundary of the process window, where stable welding is no longer reliably achieved. A comparison of the different spot diameters reveals that each produces a different gradient in weld seam width on the upper and lower sides. In all cases, however, the lower weld seam with shows a steeper gradient than the upper one. This can be attributed to heat conduction within the material. At lower welding speeds, the laser has more time to transfer heat to the second foil, leading to greater melting on the underside. When examining the difference between the upper and lower gradients for each spot size, the largest deviation is observed at a spot diameter of 48 mm (-7.17). This is followed by 124 mm (-4.46), while the smallest difference occurs at 81 µm (-2.47). These results indicate that the 81 µm spot diameter provides the most consistent relationship between upper and lower weld seam widths across varying welding speeds. It is therefore the most stable option when a minimal difference between top and bottom seam widths is required.

3.3. Weld grain structure

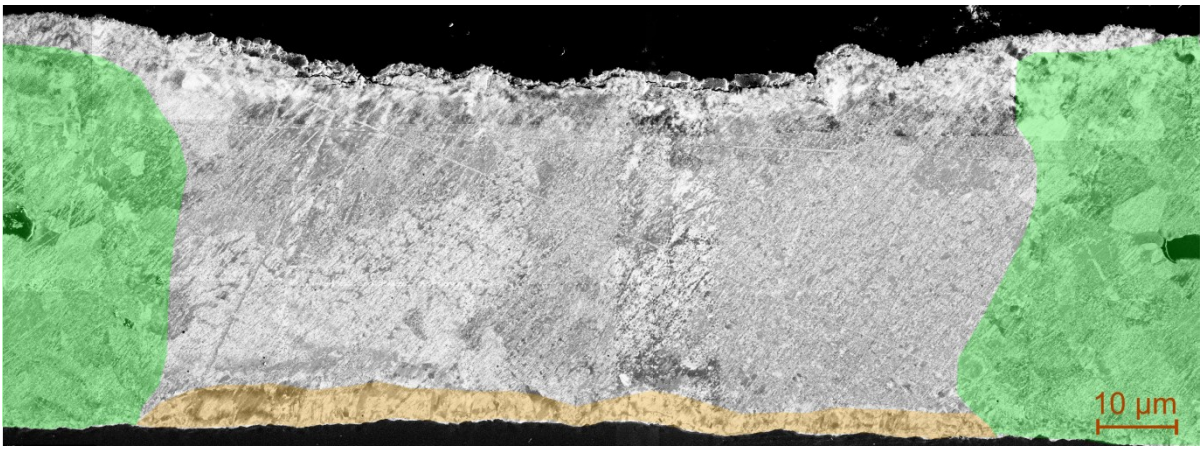

Fig. 5. Stitched ion image of weld cross-section with 81 µm spot diameter and a 11$\frac{\mathrm{mm}}{\mathrm{s}}$ welding speed

A comprehensive examination of weld seams involves not only ascertaining whether the area has been properly welded through, but also the presence of any air pockets or other anomalies within the weld seam. For this purpose, an ion image of a weld seam was taken using a FIB Strata 400 from FEI. To achieve optimal resolution, a series of small sections of a weld seam were photographed and subsequently assembled. Figure 5. shows the stiched image of a weld cross-section with a 81 µm spot diameter and a 11 millimeters per second welding speed. The presence of hard edges is notable at the upper edge and in the central region of the assembled image. This discrepancy can be attributed to the fact that multiple photographs of the weld seam were taken at these points. The upper weld seam is at the top of the picture and the lower weld seam at the bottom. At the left and right side of the image, the individual layers of the two foils are discernible, as they have not been fused together in that particular area. This is also the region where the grain structure of the bulk material is visible. For better visualization of this area the bulk grain size has been delineated in green. A distinct grain structure is also evident in the lower weld seam indicated by the orange coloration. This phenomenon can be attributed to the rapid cooling of the melt in this region due to its contact with the holder. In the center area, larger grain structures are observed in the weld seam. However, the occurrence of air bubbles during the welding process remains undetectable. In the Appendix in Figure 9 the stitched ion image is showed without the colored areas.

3.4. Heat affected zone

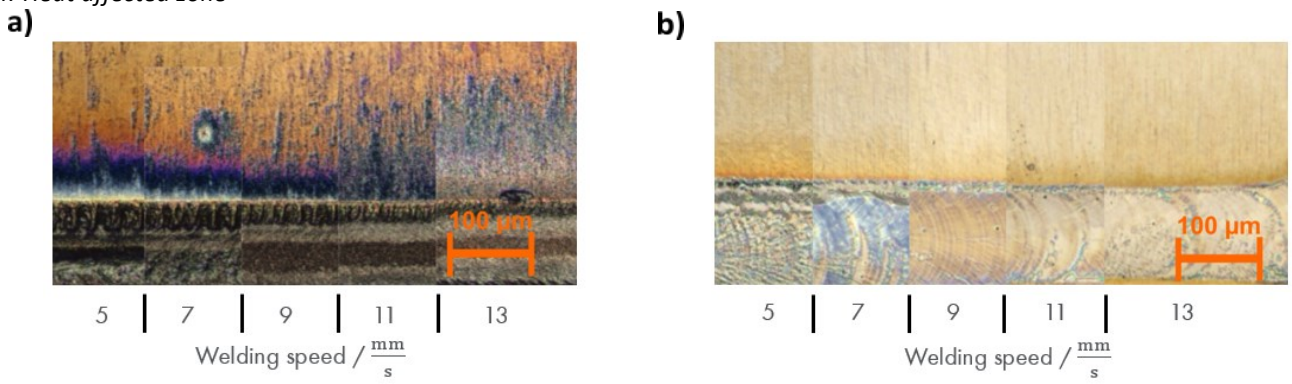

Fig. 6. a) Upper weld seam for 81 µm spot diameter at different welding speeds
b) Lower weld seam for 81 µm spot diameter at different welding speeds

The objective of welding thin metal foils necessitates a comprehensive analysis of the thermal impact on the surrounding material. This procedure must be performed on both the upper and lower welds. As shown in Figure 6 a), the upper weld for the 81 µm spot diameter is demonstrated at varying welding speeds. In order to facilitate a comparison of the heat-affected zone (HAZ), the edge of the processed material has been positioned at the same height for different welding speeds. As expected that at a rate of 5 millimeters per second, the maximum temperature is attained, as evidenced by the presence of the white annealing color along the periphery of the weld. As welding speeds increase, the width of the general HAZ and even the highest temperature are decreasing as expected. This phenomenon is evident at a welding speed of 9 millimeters per second, where the white bluish annealing color nearly disappears. In the context of the observed sequence of events, it can be posited that as welding speeds are increased, the influence of the HAZ should be decreased due to a reduction in puls overlap, leading to a decrease in heat transfer through the material. The reduction in HAZ width exhibited an interruption at an incremental rate of 11 millimeters per second. At this rate of welding, the presence of discernible annealing colors is no longer perceivable. An examination of the specimen reveals the presence of a textured area in close proximity to the weld seam . The elevated welding speed results in the ejection of molten material, which is subsequently splashed onto the periphery of the weld seam. The elevated temperature of the molten material also leads to the formation of splatter, which subsequently anneal the surface area it comes into contact with. This shows that at a welding speed of 9 millimeters per second the lowest possible heat diffusion occurs. A comparison of the lower weld seam with the surrounding foil reveals the absence of annealing colors or molten splatter.

4. Conclusion and outlook

This study examined the parameters that can be employed for the purpose of overlap welding a 20 µm thick stainless steel foil. A welding heat map was utilized to identify potential parameters sets for welding. The parameters were examined and evaluated in terms of welding quality using a cross-section cut of the welded area. The relationship between the upper and lower weld seams was also investigated, and showed that with a spot diameter of 81 µm the optimum ration between upper and lower weld width is reached. The use of a composite ion image facilitated the verification of uniform welding without the presence of air pockets within the weld seam. The heat affected zone created by the welding was examined, and changes in velocity dependence were identified, which shows that at 9 millimeters per second the smallest HAZ is observed.

In the future, experiments on thin foils are planned for the purpose of studying their interaction with surfaces that have already undergone functionalization. The development of system technology to facilitate the use of pipe diameters measuring less than 10 millimeters is also a planned initiative.

Acknowledgements

We acknowledge the German research foundation for funding project number 467661067

References

[1] Sadeghian, A., Iqbal, N., 2022., A review on dissimilar laser welding of steel-copper, steel-aluminum, aluminum-copper, and steel-nickel for electric vehicle battery manufacturing, Optics & Laser Technology, Volume 146, p 107595.
[2] Amanat, N., James, N., McKenzie, D., 2010., Welding methods for joining thermoplastic polymers for the hermetic enclosure of medical devices, Medical Engineering & Physics, Volume 32, Issue 7, p. 690-699.
[3] Grabmann, S., Kriegler, J., Harst, F. et al., 2022 Laser welding of current collector foil stacks in battery production–mechanical properties of joints welded with a green high-power disk laser, IntJAdv ManufTechnol, 118, p.2571-2586.
[4] Boglea, A., Olowinsky, A., Gillner, A., 2007, Fibre laser welding for packaging of disposable polymeric microfluidic-biochips, Applied Surface Science, Volume 254, Issue 4, p. 1174-1178.
[5] Richter, S., Zimmermann, F., Tünnermann, A., Nolte, S., 2016, Laser welding of glasses at high repetition rates – Fundamentals and prospects, Optics & Laser Technology, Volume 83, p. 59-66
[6] Wang, Y., Li, Y., Ao, S., Lup, Z., Zahng, D., 2021, Welding of 304 stainless steel an glass using high-repetition-frequency demtosecond laser

Appendix A.

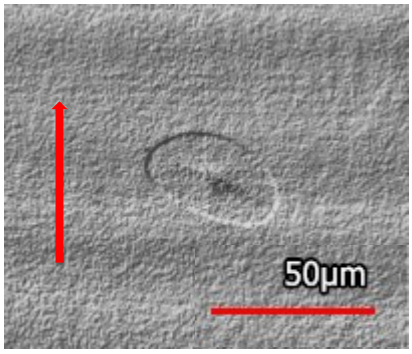

Fig. 7. Single pulse on silicon with a pulse energy of 19 µJ at z = -4 mm (Arrow indicates the scan direction).

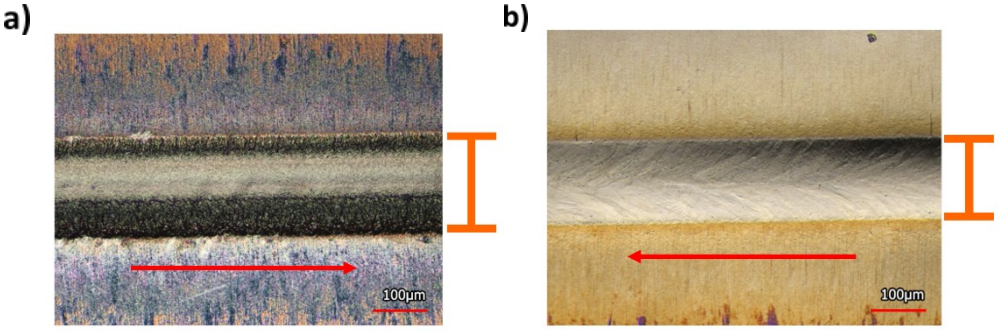

Fig. 8. a) Upper welding seam with 124 µm spot diameter and a 13$\frac{\text{mm}}{\text{s}}$ welding speed (Arrow indicates the scan direction).
b) Lower welding seam with 124 µm spot diameter and a 13$\frac{\text{mm}}{\text{s}}$ welding speed (Arrow indicates the scan direction).

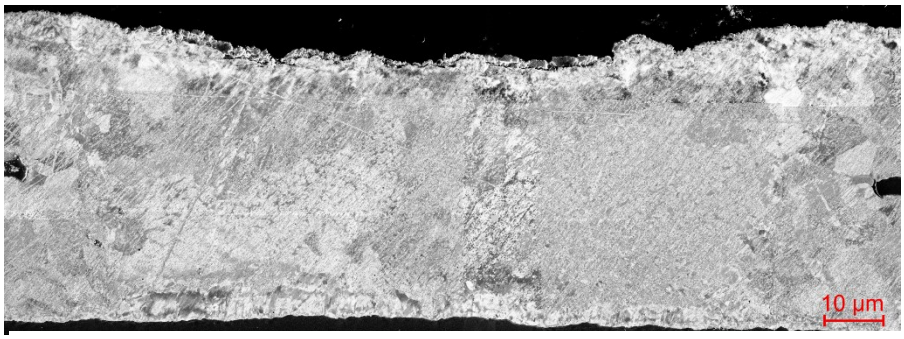

Fig. 9. Stitched ion image of weld cross-section with 81 µm spot diameter and a 11$\frac{\text{mm}}{\text{s}}$ welding speed